Supplemental Information

A new site of broad vulnerability on the HIV-1 envelope spike defined by antibody 8ANC195

Louise Scharf[1], Johannes F. Scheid[2†], Jeong Hyun Lee[3†], Anthony P. West, Jr.[1], Courtney Chen[1], Han Gao[1], Priyanthi N.P. Gnanapragasam[1], René Mares[1], Michael S. Seaman[4], Andrew B. Ward[3], Michel C. Nussenzweig[2,5], Pamela J. Bjorkman[1,5*]

[1] Division of Biology and Biological Engineering, California Institute of Technology, 1200 E. California Blvd., Pasadena, CA 91125, USA

[2] Laboratory of Molecular Immunology, The Rockefeller University, New York, NY 10065, USA

[3] Department of Integrative Structural and Computational Biology, The Scripps Research Institute, La Jolla, CA 92037, USA

[4]Beth Israel Deaconess Med. Ctr., Boston, MA 02215; United States

[5] Howard Hughes Medical Institute

† These authors contributed equally.

* Corresponding author

Figure S1, Related to Figure 1

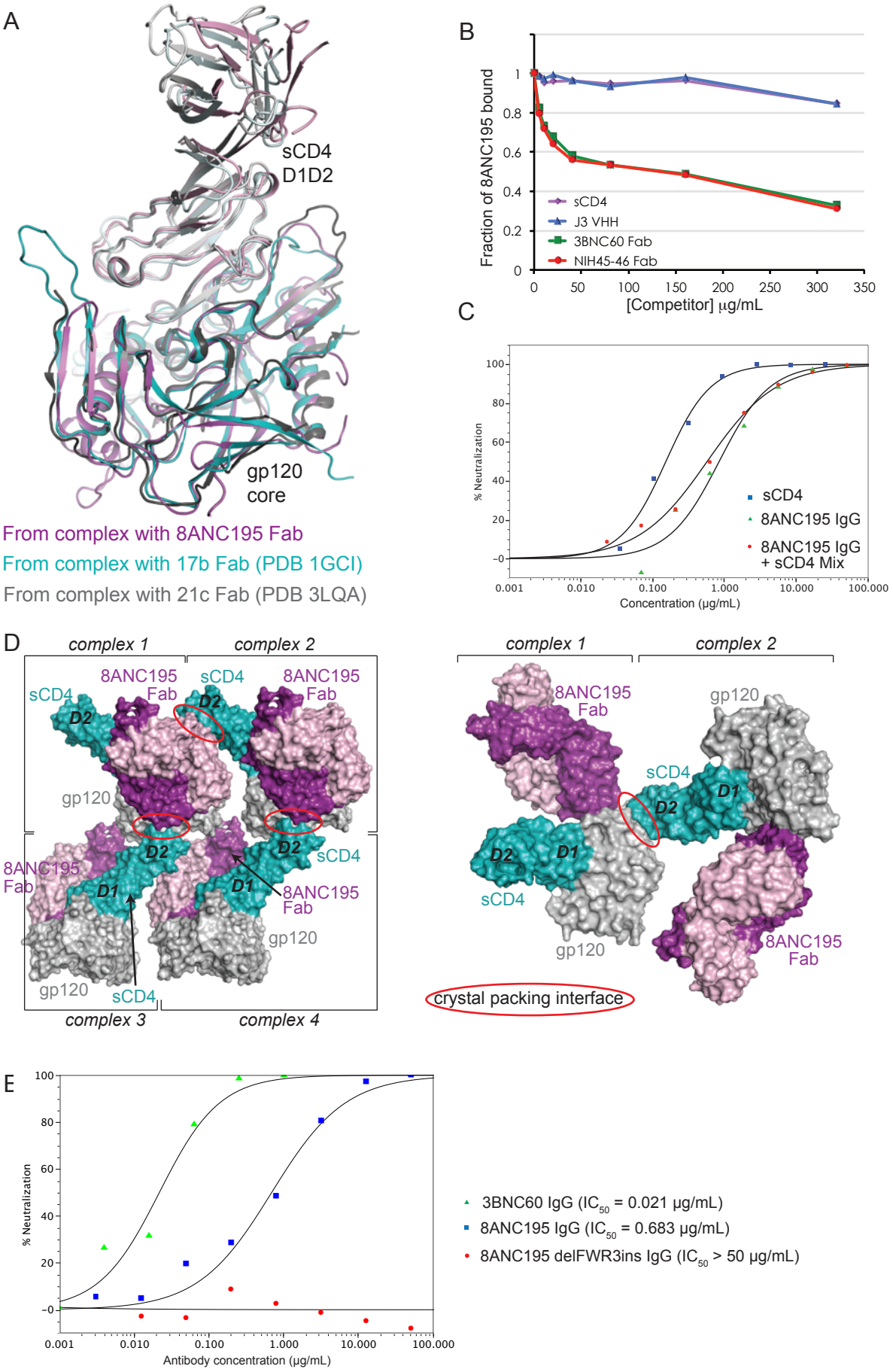

Supplemental Figure 1, Related to Figure 1. sCD4 interactions with 8ANC195. (A) Superimposition of sCD4 D1D2/gp120 structures (ribbon diagrams) from complexes with 8ANC195 (purple), 17b (cyan, PDB 1GCI) and 21c (grey, PDB 3LQA). (B) Competition ELISA of 8ANC195 IgG binding to 93TH057 gp120 in the presence of increasing concentrations of potential competitors (sCD4, purple diamonds; J3 VHH, blue triangles; 3BNC60 Fab, green squares; NIH45-46 Fab, red circles). No competition was observed with small, single-Ig domain CD4-binding site ligands (sCD4, J3 VHH), but larger Fab fragments of CD4 binding site antibodies (3BNC60, NIH45-46) competed for binding. (C) *In vitro* assay comparing neutralization of YU2 by sCD4 (blue squares), 8ANC195 IgG (green triangles), and an equimolar mixture of 8ANC195 and sCD4 (red circles). (D) Packing of 8ANC195/sCD4/gp120 crystals. Several symmetry mates are shown as surface representations (8ANC195 HC, purple; 8ANC195 LC, pink; 93TH057 gp120, grey; sCD4 D1D2, cyan). Areas where two complexes form crystal contacts are indicated with red circles. (E) *In vitro* assay comparing neutralization of YU2 by 8ANC195 IgG (blue squares), 3BNC60 IgG (green triangles), and an 8ANC195 IgG mutant that lacks the FWR3 insertion (Ser77a-Pro77b-Pro77c-Ile77d) that results in the protruding "$FWR3_{HC}$ thumb" (red circles).

Figure S2, Related to Figure 3

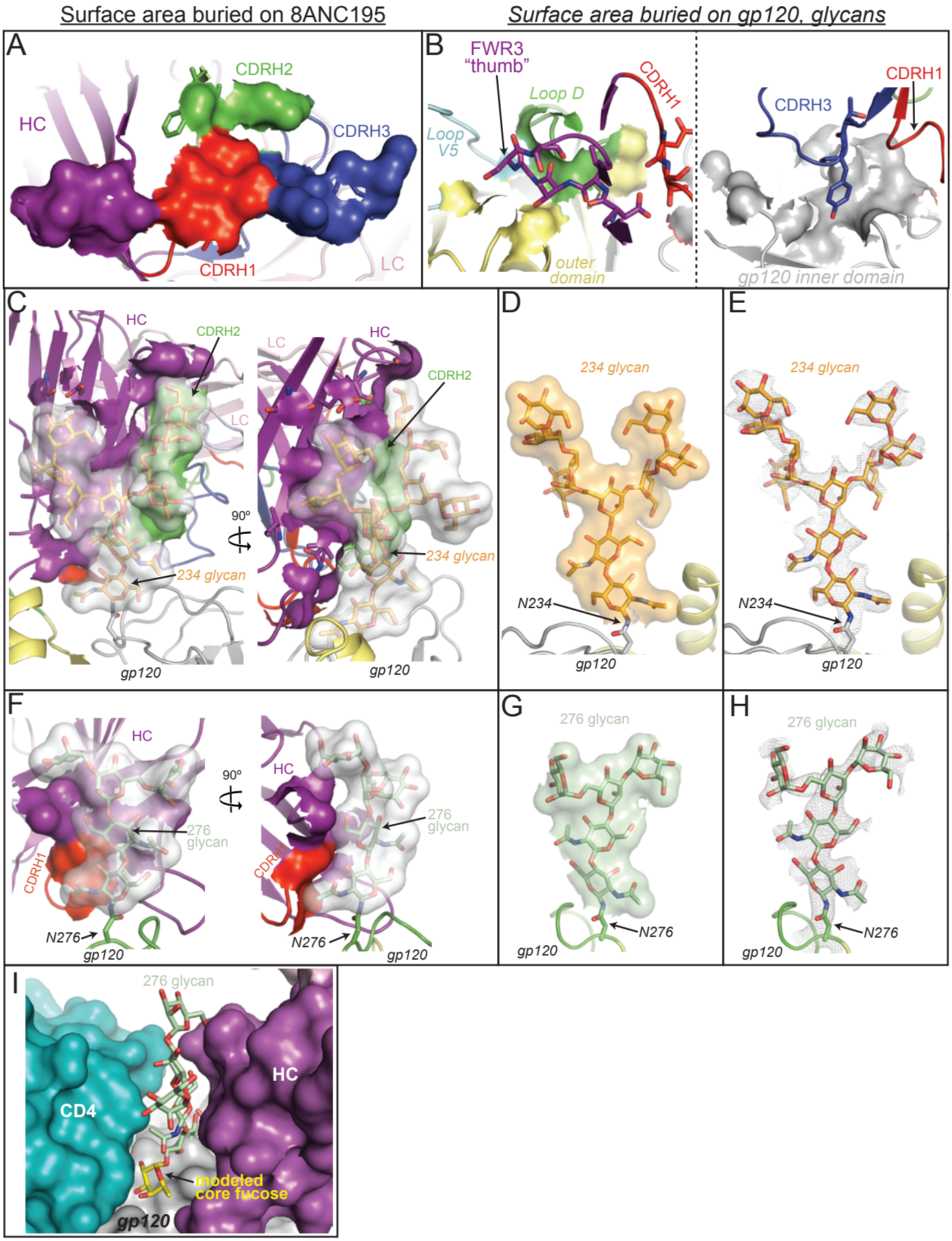

Supplemental Figure 2, Related to Figure 3. Surface area buried at interface of 8ANC195 Fab and gp120. Left panels, surface area buried on 8ANC195 Fab by (A) gp120 protein residues, (C) $Asn234_{gp120}$ glycan or (F) $Asn276_{gp120}$ glycan; right panels, surface area buried by 8ANC195 Fab on (B) gp120 protein residues, (D) $Asn234_{gp120}$ glycan or (G) $Asn276_{gp120}$ glycan. Atoms buried at these interfaces are shown as surface representations overlaid onto ribbon diagrams of 8ANC195 Fab and gp120 or stick representations of glycans. 8ANC195 Fab: HC, purple; LC, pink; CDRH1, red; CDRH2, green; CDRH3, blue; gp120: inner domain, grey; outer domain, light yellow; loop D, green; loop V5, cyan; $Asn234_{gp120}$ glycan: orange; $Asn276_{gp120}$ glycan: light green. 2Fo-Fc annealed omit electron density maps (grey mesh, σ=1) used to build (E) $Asn234_{gp120}$ glycan and (H) $Asn276_{gp120}$ glycan. (I) Modeled fucose residue (yellow) α1-6-linked to the first *N*-acetylglucosamine residue of the $Asn276_{gp120}$ glycan shows that the core fucose of a complex-type *N*-glycan could be accommodated by the 8ANC195. Glycan residues are shown as sticks, and gp120 (grey), 8ANC195 HC (purple) and CD4 (teal) are shown as surface representations.

Figure S3, Related to Figure 5

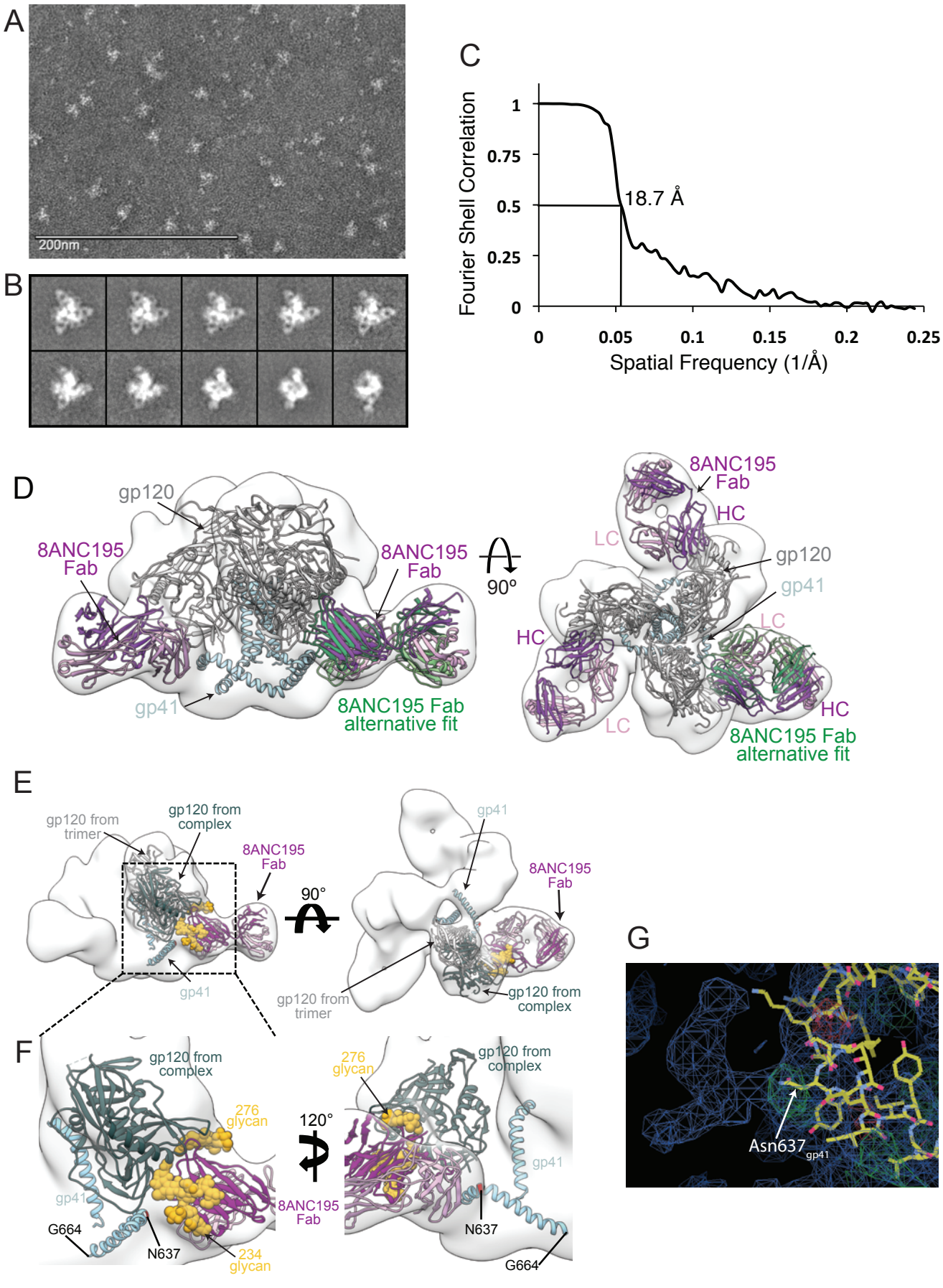

Supplemental Figure 3, Related to Figure 5. EM refinement statistics and negative stain EM reconstructions. (A) Electron micrograph at 52,000x magnification and -0.8 μm defocus. (B) Reference-free 2D class averages of the SOSIP trimer in complex with 8ANC195 Fab showing various orientations. In each of the class averages the Fabs were easily identified. (C) The resolution was determined as 18.7 Å at a Fourier Shell Correlation (FSC) cut-off of 0.5. (D) EM reconstruction of 8ANC195 Fab/BG505 SOSIP.664. Side (left) and top (right) views of EM density with the X-ray structures of BG505 SOSIP.664 (PDB ID 4NCO; gp120, grey; gp41, light blue) and 8ANC195 Fab fit in two ways: (i) fitting 8ANC195 Fab independently of gp140 coordinates to the EM density (best fit/independently placed) (purple), and (ii) by aligning the gp120 of the gp120/8ANC195 complex structure onto the gp120 of PDB 4NCO fit to the EM density (green). (E) When the gp120-8ANC195 Fab structure was fit into the EM density, the gp120 from the complex structure (dark green) was displaced slightly outwards in comparison to the gp120 in the SOSIP trimer structure (grey). The HC and LC of the Fab are shown in magenta and in pink, respectively. The $Asn234_{gp120}$ and $Asn276_{gp120}$ glycans are shown as yellow spheres. (F) Close up of the Fab-Env interface resulting from the independent docking. The position of $Asn637_{gp120}$ (red) can be deduced from the position of the C-terminus of HR2, which corresponds to residue $Gly664_{gp41}$. This residue is in close proximity to the LC and the glycan at this position could interact with the 8ANC195 Fab. The coloring scheme is as in D. Docking of the gp120-8ANC195 portion of the ternary crystal structure onto the SOSIP trimer structure resulted in a slightly different angular placement of the Fab in the EM density than when the 8ANC195 Fab was fit independently. The Fab, especially the LC, was pushed further away from gp41 in comparison to the placement suggested by the complex crystal structure. The LC position in the independently-fit EM model was more likely to be accurate since it left space for bulky side chains at positions 625_{gp41}-640_{gp41} that were modeled as alanines in the trimer crystal structure (Julien et al., 2013; Lyumkis et al., 2013). The slightly different placements could be due to crystal packing effects, spatial restraints imposed by the gp41

glycans that were not present in the 8ANC195-gp120 complex, removal of the PNGS at $Asn88_{gp120}$ in the gp120 core, which may have allowed for a closer association of 8ANC195 and gp120 in the crystal structure, and/or a small conformational change in the gp120 region of the trimer to accommodate the Fab orientation trapped by crystallization, potentially to accommodate the $Asn611_{gp41}$ and $Asn637_{gp41}$ glycans. (G) 2Fo-Fc electron density map (blue, σ=1) calculated using 4NCO structure factors and 4NCO coordinates. Positive and negative densities from an Fo-Fc map shown in green and red, respectively (σ=2.5). Side chains for the BG505 HR2 helix were modeled into the polyalanine 4NCO coordinates in this region. The modeled sidechains and the $Asn637_{gp41}$ glycan were not included in the model from which calculated structure factors (Fc) were derived.

Figure S4, Related to Figure 5

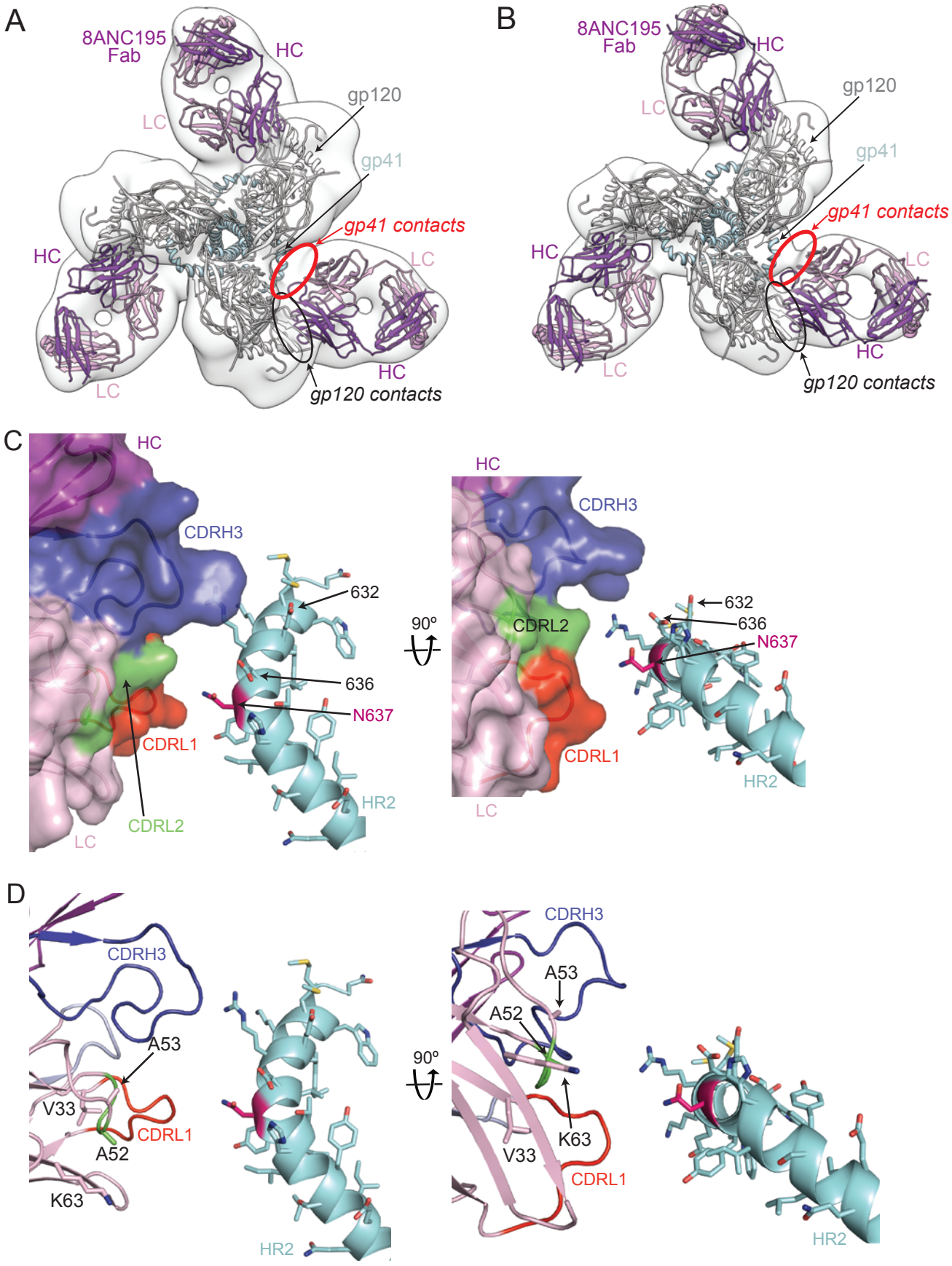

Supplemental Figure 4, Related to Figure 5. EM reconstruction of 8ANC195 Fab/BG505 SOSIP.664 complex showing gp41 contacts. Top view of EM density with the X-ray structures of BG505 SOSIP.664 (PDB ID 4NCO; gp120, grey; gp41, light blue) and 8ANC195 Fab (HC, purple; LC, pink) with a map contour level of 0.0176 (A) and 0.030 (B). Areas of contact between 8ANC195 and gp41 are marked with red circles, those between 8ANC195 and gp120 with black circles. (C,D) Close-up of 8ANC195 LC and HR2 region in EM complex structure (HR2 coordinates in PDB 4NCO with presumptive sidechains for strain YU2 added to the polyalanine coordinates). (C) Fab is shown as a surface representation with highlights (CDRL1, red; CDRL2, green; CDRH3, blue), and gp41 HR2 is shown as a ribbon diagram (light blue). The position of $Asn637_{gp41}$ (magenta) was deduced from the position of the C-terminus of the SOSIP.664 trimer ($Gly664_{gp41}$). (D) 8ANC195 HC and LC residues (sticks) positioned to contact HR2, with side chains of surface-exposed residues that vary between newly isolated 8ANC195 (γ/κ) variants shown as sticks.

Figure S5, Related to Figure 6

A

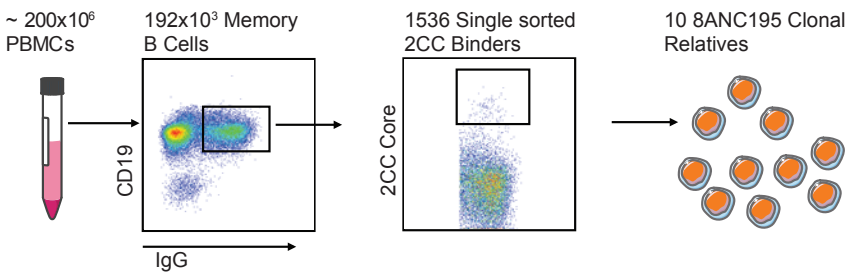

B

Heavy Chains

Ab name	VH	D	JH	(-)	CDR3 (aa)	(+)	Length	Mutations HC
8ANC195	1-69	3-3	ND	2	T S T Y D K W S G L H H D G V M A F S S	3	20	73
8ANC2080	1-69	3-3	ND	2	T S T Y D K W S G L H H D G V M A F S S	3	20	73
8ANC3035	1-69	3-3	ND	2	T S T Y D K W S G L H H D G V M A F S S	3	20	73
8ANC3369	1-69	3-3	ND	2	T S T Y D K W S G L H H D G V M A F S S	3	20	73
8ANC3625	1-69	3-3	ND	2	T S T Y D K W S G L H H D G V M A F S S	3	20	73
8ANC142	1-69	3-3	ND	2	T S T Y D Q W S G L H H D G V M A F S S	2	20	72
8ANC3040	1-69	3-3	ND	2	T S T Y D Q W S G L H H D G V M A F S S	2	20	72
8ANC3288	1-69	3-3	ND	2	T S T Y D Q W S G L H H D G V M A F S S	2	20	72
8ANC3430	1-69	3-3	ND	2	T S T S D Y W S G L H H D G V M A F S S	2	20	71
8ANC3484	1-69	3-3	ND	2	T S T Y D R W S G L H H D G V M A F S S	3	20	75
8ANC3044	1-69	3-3	ND	2	T S T Y D K W S G L H H D G V M A F S S	3	20	74
8ANC3630	1-69	3-3	ND	2	T S T Y D R W S G L H H D G V M A F S S	3	20	82

Light Chains

Ab name	k/l	Vk/l	Jk/l	(-)	CDR3 (aa)	(+)	Length	Mutations LC	NEUT
8ANC195	k	1-5	1/5	1	Q Q Y D T Y P G T	0	9	41	+
8ANC2080	k	1-5	1/5	1	Q Q Y D T Y P G T	0	9	41	+
8ANC3035	k	1-5	1/5	1	Q Q Y D T Y P G T	0	9	41	+
8ANC3369	k	1-5	1/5	1	Q Q Y D T Y P G T	0	9	41	+
8ANC3625	k	1-5	1/5	1	Q Q Y D T Y P G T	0	9	41	+
8ANC142	k	1-5	1/5	1	Q Q Y D T Y P G T	0	9	43	+
8ANC3040	k	1-5	1/5	1	Q Q Y D T Y P G T	0	9	43	+
8ANC3288	k	1-5	1/5	1	Q Q Y D T Y P G T	0	9	43	+
8ANC3430	k	1-5	1/5	1	Q Q Y D T Y P G T	0	9	38	+
8ANC3484	k	1-5	1/5	1	Q Q Y D T Y P G T	0	9	42	+
8ANC3044	k	1-5	1/5	1	Q Q Y D T Y P G T	0	9	40	+
8ANC3630	k	1-5	1/5	1	Q Q Y D T Y P G T	0	9	40	+

C

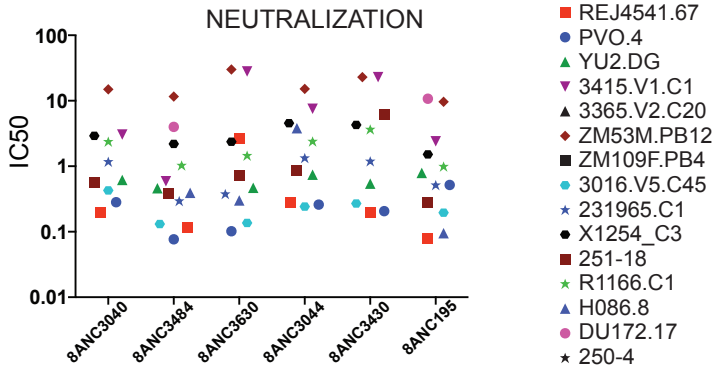

D ***HC***

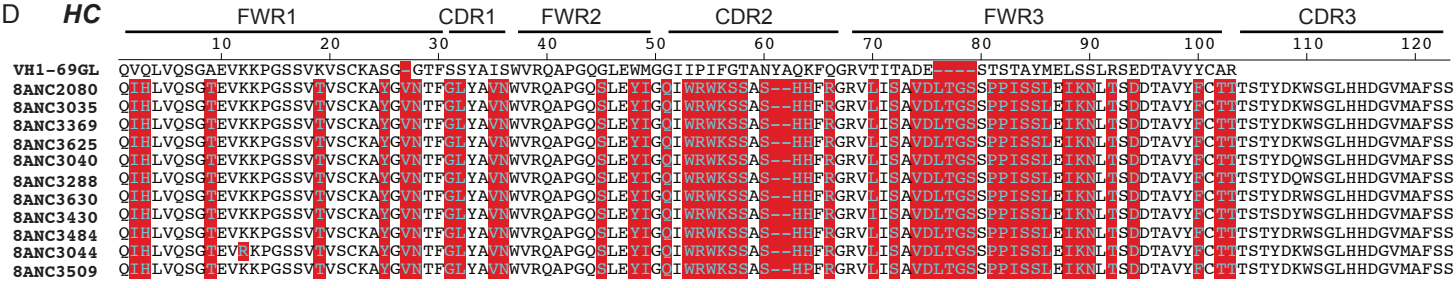

E ***LC***

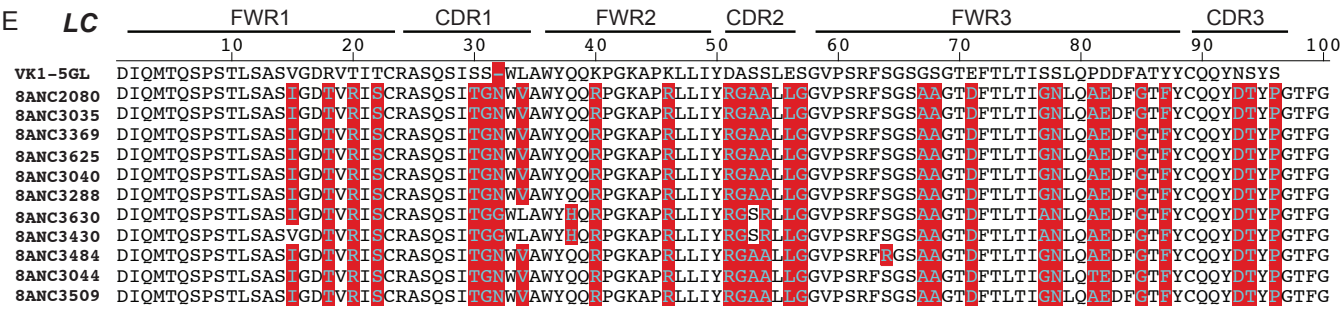

Supplemental Figure 5, Related to Figure 6. Single Cell Variants of 8ANC195. (A) Strategy of large scale single cell sorting. (B) IgH and IgL chain genes from isolated single cell variants of 8ANC195. Identical members are grouped together. (C) IC_{50} neutralization titers of distinct single cell versions of the 8ANC195 clone compared to 8ANC195 against a 15 virus Tier 2 panel. (D) HC and (E) LC sequences were aligned with the respective germline genes. Mutations introduced by somatic hypermutation are shown in red.

Figure S6, Related to Figure 6

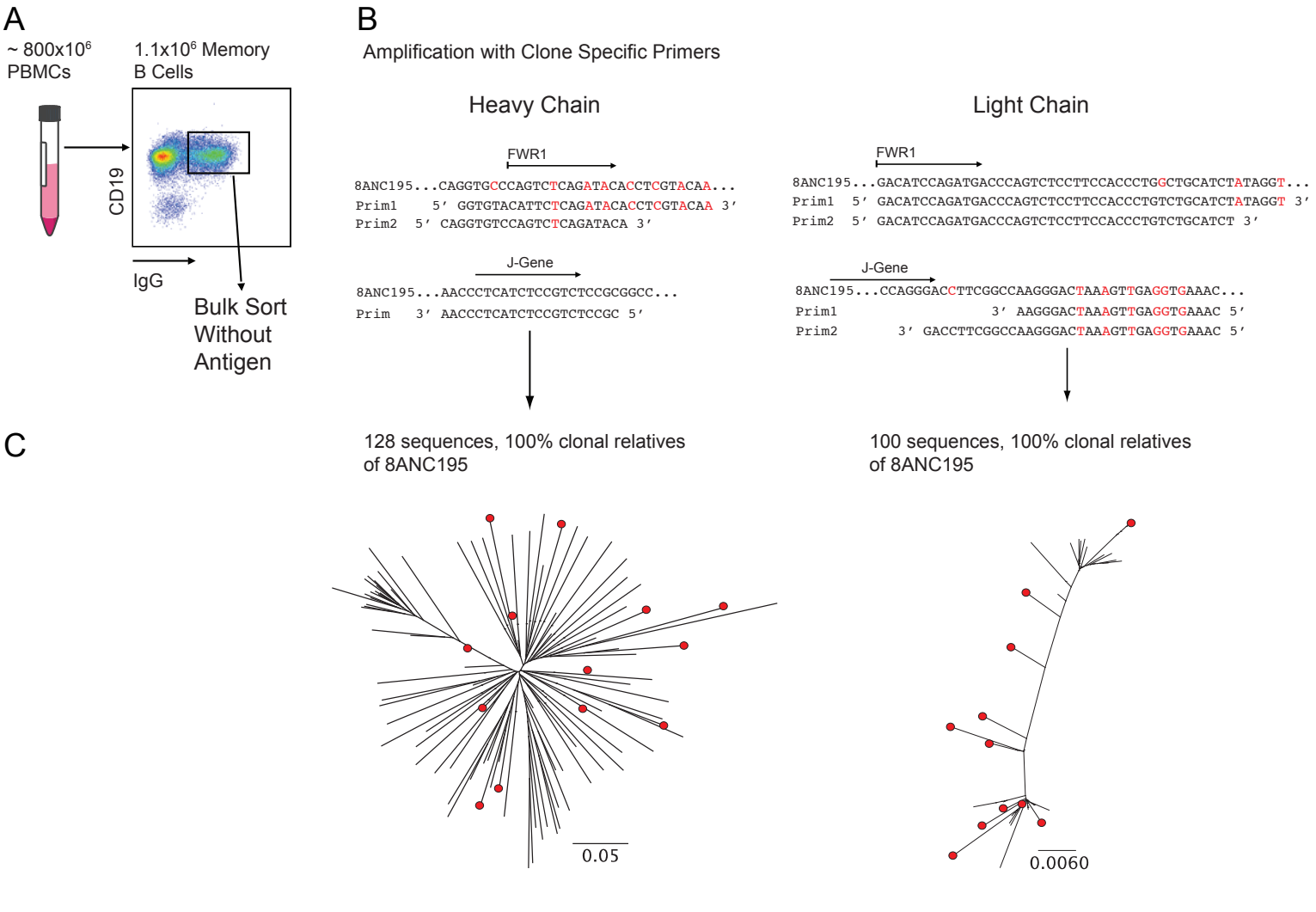

Supplemental Figure 6, Related to Figure 6. Bulk Sorted Variants of 8ANC195. (A) Strategy of bulk memory B cell sorting without antigen. (B) PCR strategy for the amplification of 8ANC195 HC and LC clone members. Shown are the priming sites aligned with the original nucleotide sequence of 8ANC195 at the respective sites. Mismatches with the respective germline genes are marked in red. (C) Phylogenetic tree of 128 isolated HC and 100 LC sequences. Representative members chosen for alignment are marked in red. (D) HC and (E) LC sequences were aligned with the respective germline genes as well as the original 8ANC195 sequence. All mutations introduced by somatic hypermutation are shown in red.

Figure S7, Related to Figure 6

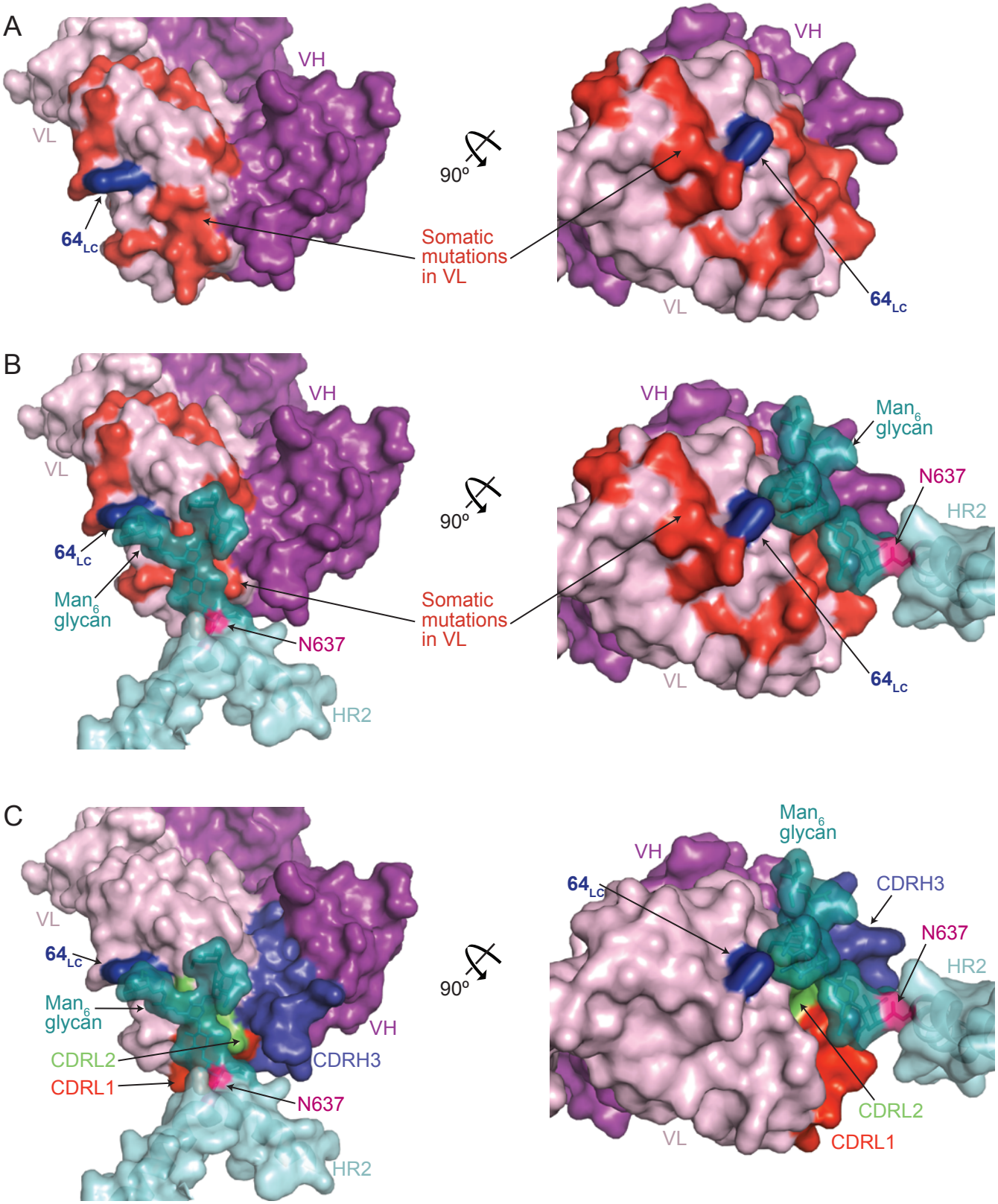

Supplemental Figure 7, Related to Figure 6. Somatic mutations in the 8ANC195 LC CDRs and FWRs could affect contacts with gp41. (A) Surface representation of 8ANC195 Fab (HC, purple; LC, light pink; somatically mutated, surface-exposed LC residues, red; residue 64_{LC}, dark blue). (B) Surface representation of 8ANC195 Fab (coloring as in A) and BG505 gp41 HR2 (cyan) with a modeled Man_6 sugar (teal) attached to $Asn637_{gp41}$ (magenta). (C) Surface representation of 8ANC195 Fab (CDRL1, red; CDRL2, green; CDRH3, blue; residue 64_{LC}, dark blue) and BG505 gp41 HR2 (cyan) with a modeled Man_6 sugar (teal) attached to $Asn637_{gp41}$ (magenta).

Table S1. Data collection and refinement statistics, molecular replacement, Related to Figure 1.

	8ANC195 Fab/gp120/sCD4 complex	8ANC195 Fab
Data collection		
Resolution range (Å)	39.22 - 3.0 (3.22 - 3.0)	29.73 - 2.13 (2.21 - 2.13)
Space group	P 2_1 2_1 2_1	P 4_1 2_1 2
Cell dimensions		
a, b, c (Å)	66.53, 132.49, 142.77	66.48, 66.48, 219.03
α, β, γ (°)	90, 90, 90	90, 90, 90
Total reflections	229212 (12539)	239217 (24708)
Unique reflections	36730 (3064)	28097 (2788)
Multiplicity	6.2 (6.3)	8.4 (8.9)
Completeness (%)	97.65 (99.80)	98.92 (91.00)
Mean I/σ(I)	7.86 (2.1)	11.90 (3.16)
Wilson B-factor	61.95	32.47
R_{merge}	0.1747 (0.765)	0.1225 (0.5802)
CC1/2	0.998 (0.854)	0.996 (0.876)
CC*	0.999 (0.960)	0.999 (0.966)
Refinement		
R_{work}/R_{free}	0.235/0.272	0.202/0.242
Number of atoms	7603	3514
Protein	7195	3321
Ligands	408	15
Water	0	178
R.m.s. deviations		
Bond lengths (Å)	0.011	0.010
Bond angles (°)	1.1	1.23
Average B-factor		
Protein	66.8	36.9
Ligands	89.7	54.0
Water	-	43.4

Statistics for the highest-resolution shell are shown in parentheses.

Table S2. Table of contacts between gp120 and 8ANC195 in complex crystal structure, Related to Figure 3.

Buried Surface Area (BSA) at Interfaces			
gp120	**BSA (Å^2)**	**8ANC195 HC**	**BSA (Å^2)**
VAL 44	18.4	ASN 28	29.0
TRP 45	18.2	THR 29	23.8
LYS 46	37.2	GLY 31	22.6
ASP 47	33.2	LEU 32	60.8
VAL 89	4.5	ARG 54	64.0
THR 90	39.8	TRP 55	3.8
GLU 91	12.3	LYS 56	2.2
ASN 92	90.3	ASP 73	3.1
PHE 93	6.1	LEU 74	62.8
ASN 94	33.9	THR 75	52.7
LYS 97	5.7	GLY 76	82.6
ASN 234	3.2	SER 77	39.2
THR 236	43.3	SER 77a	6.2
GLY 237	18.9	PRO 77b	4.1
PRO 238	56.8	THR 97	9.4
LYS 240	2.2	TYR 98	98.0
GLU 275	11.2	ASP 99	13.5
ASN 276	17.3	LYS 100	34.5
LEU 277	33.8	TRP 100a	72.2
THR 278	68.1		
HIS 352	19.3		
PHE 353	10.6		
ASN 354	44.3		
LYS 357	8.5		
ARG 456	14.5		
THR 463	4.7		
GLU 466	0.5		
LYS 487	5.8		
Total gp120	662.5	Total 8ANC195 HC	684.4

Hydrogen Bonds at Interfaces				
gp120		**8ANC195 HC**		**Distance (Å)**
THR 278	Oγ1	THR 75	O	2.35
ARG 456	NH2	GLY 76	O	3.06
ASN 354	Oδ2	SER 77	Oγ	3.11
THR 278	Oγ1	SER 78	O	3.29
ASN 92	Nδ2	THR 104	O	3.00
ASN 92	Nδ2	TYR 105	O	3.00
HIS 352	O	THR 75	Oγ1	2.99
ASN 354	Oδ1	THR 75	Oγ1	3.36
ASP 47	Oδ2	TYR 105	OH	2.78
LYS 487	Nζ	TYR 105	OH	3.37

gp120	BSA (Å^2)	8ANC195 HC	BSA (Å^2)
gly276 NAG[1]	121.0	TYR 25	12.01
		GLY 26	40.84
		VAL 27	5.02
		ASN 28	14.88
		LEU 74	19.84
		PRO 77b	3.51
gly276 NAG[2]	105.7	GLN 1	20.19
		HIS 3	5.04
		TYR 25	38.48
		GLY 26	13.63
gly276 BMA[3]	76.5	GLN 1	4.92
		HIS 3	35.32
		VAL 5	9.05
		TYR 25	20.18
gly276 MAN[4]	74.1	GLN 1	13.78
		ILE 2	5.4
		HIS 3	41.88
gly276 MAN[5]	39.9	VAL 5	15.89
		TYR 25	17.71
Total gly276	417.2	Total 8ANC195 HC	337.6

Table S2. Cont'd.

Buried Surface Area (BSA) at Interfaces			
gp120	**BSA (Å^2)**	**8ANC195 HC**	**BSA (Å^2)**
gly234 NAG[1]	107.1	ASN 28	1.6
		THR 29	6.03
		TRP 55	23.63
		ASP 73	35.3
		LEU 74	16
gly234 NAG[2]	132.3	ARG 54	1.84
		TRP 55	48.51
		ALA 71	3.57
		VAL 72	12.65
		ASP 73	13.11
gly234 BMA[3]	104.0	ILE 52	7.35
		TRP 55	23.33
		ALA 57	4.89
		SER 70	11.07
		ALA 71	12.3
		VAL 72	11.21
gly234 MAN[4]	59.7	SER 70	9.64
		ALA 71	6.02
		VAL 72	30.04
gly234 MAN[5]	126.6	THR 19	0.5
		SER 70	11.18
		ALA 71	3.14
		VAL 72	18.58
		ILE 77d	17.52
		SER 78	0.16
		SER 79	16.85
gly234 MAN[6]	122.4	THR 19	20.36
		LEU 68	25.6
		SER 70	8.5
		SER 79	7.06
		GLU 81	21.78
gly234 MAN[7]	87.1	ILE 51	2.5
		TRP 55	12.34
		LYS 56	1.68
		ALA 57	20.4
		LEU 68	16.83
		ILE 69	1.47
		SER 70	4.77
gly234 MAN[8]	64.4	ALA 57	24.52
		SER 58	2.01
		LEU 68	23.58
gly234 MAN[10]	207.3	ALA 57	15.4
		SER 58	13.36
		ALA 59	17.51
		ARG 64	13.1
		GLY 65	11.32
		VAL 67	11.98
		LEU 68	7.87
		ILE 69	4.34
Total gly234	1010.8	Total 8ANC195 HC	554.8

Hydrogen Bonds at Interfaces				
gp120		**8ANC195 HC**		**Distance (Å)**
gly234 NAG[1]	O4	TRP 55	Nε1	3.06
gly234 NAG[1]	N2	ASP 73	Oδ2	2.73
gly234 NAG[2]	O6	ASP 73	N	3.01
gly234 MAN[5]	O6	SER 79	Oγ	2.78
gly234 MAN[5]	O5	SER 70	Oγ	3.47
gly234 MAN[6]	O3	THR 19	Oγ1	3.35
gly234 MAN[10]	O2	ALA 59	N	3.29
gly234 MAN[10]	O4	GLY 65	N	3.32
gly234 MAN[10]	O6	ILE 69	N	2.84
gly234 MAN[10]	O6	SER 57	Oγ	2.35
gly234 MAN[10]	O5	SER 57	Oγ	3.28

Table S3. Affinity constants and neutralization potency of 8ANC195 light chain chimera antibodies, Related to Figure 6.

	K_D (nM)		IC_{50} (μg/mL)									
Antibody	93TH057 gp120	YU2 gp120	YU2	Tro11	SF162	6535_3	SC4226618	PVO4	RHPA4259	TRJO 4551	DU156	REJO4541
8ANC195	33.1	82.0	0.4	0.31	0.30	0.43	0.69	0.52	0.17	0.46	0.54	0.21
8ANC195 mHC/glLC1	38.0	56.1	6.76	>100	12.9	8.9	8.1	11.5	14.6	ND	ND	>100
8ANC195 glCDRL1	38.0	105.4	55	>100	65	24	97	>100	0.96	>100	8.1	>100
8ANC195 glCDRL2	40.5	119.5	6.26	18.9	44	13.3	69	97	0.82	>100	>100	>100
8ANC195 glCDRL3	44.4	107.1	0.79	0.75	0.85	1.08	1.29	3.1	0.97	23	0.22	1.56
8ANC195 CDRL3Ala	ND	ND	39	ND	>100	>100	>100	>100	0.81	>100	ND	ND
8ANC195HC/ 3BNC117LC	ND	ND	4.77	5.33	5.6	>100	22	ND	4.52	18	ND	3.25
3BNC60	ND	ND	0.027	0.04	0.05	0.335	0.07	0.06	0.02	0.18	0.013	0.063
8ANC195 DFWR3insert	ND	ND	>50	ND	ND	ND	ND	ND	ND	ND	ND	ND

	IC_{50} (μg/mL)
Antibody	YU2 N637Q
8ANC195	0.574
3BNC60	0.018

IC_{50} < 0.1 μg/mL

IC_{50} 0.1 - 1 μg/mL

IC_{50} 1.1 - 5 μg/mL

IC_{50} 5.1 - 20 μg/mL

IC_{50} 20.1 - 100 μg/mL

Supplementary Table 4, Related to Figure 6.

Virus	8ANC3040	8ANC3484	8ANC3630	8ANC3044	8ANC3430	8ANC195
REJO4541.67	**0.198**	**0.117**	**2.652**	**0.278**	**0.198**	**0.08**
PVO.4	**0.284**	**0.077**	**0.102**	**0.260**	**0.206**	**0.52**
YU2.DG	**0.617**	**0.461**	**0.468**	**0.747**	**0.545**	**0.79**
3415.v1.c1	**3.059**	**0.589**	**27.977**	**7.557**	>23	**2.404**
3365.v2.c20	>25	>30	>30	>30	>23	>30
ZM53M.PB12	**14.910**	**11.581**	>30	**15.164**	>23	**9.626**
ZM109F.PB4	NT	>30	>30	>30	>23	>30
3016.v5.c45	**0.427**	**0.131**	**0.136**	**0.242**	**0.271**	**0.195**
231965.c1	**1.174**	**0.294**	**0.375**	**1.332**	**1.190**	**0.514**
X1254_c3	**2.909**	**2.192**	**2.377**	**4.538**	**4.284**	**1.524**
251-18	**0.571**	**0.391**	**0.730**	**0.858**	**6.170**	**0.284**
R1166.c1	**2.370**	**1.027**	**1.453**	**2.381**	**3.642**	**0.986**
H086.8	NT	**0.394**	**0.300**	**3.830**	>23	**0.095**
Du172.17	NT	**4.011**	>30	>30	>23	**10.797**
250-4	NT	>30	>30	>30	>23	>50
MuLV	>30	>30	>30	>30	>23	>23

Neutralization activity of single sorted clonal members of 8ANC195. IC_{50} neutralization titers (μg/mL) of 5 distinct clonal relatives of 8ANC195 are shown against a 15 Tier 2 virus panel. MuLV, murine leukemia virus control.

Supplemental Table 5, Related to Figure 6. Neutralization activity of bulk sorted clonal members of 8ANC195. (Submitted as Excel file)

Supplemental Experimental Procedures

Crystallization

Crystallization conditions were screened using vapor diffusion in sitting drops set using a Mosquito® crystallization robot (TTP labs) in a final volume of 200 nL per drop (1:1 protein to reservoir ratio) utilizing commercially available crystallization screens (Hampton Research, Microlytic). Initial crystallization hits for 8ANC195 Fab and for 8ANC195 Fab/93TH057 gp120/sCD4$_{K75T}$ complex were identified using the MCSG-1 (Microlytic) and PEGRx (Hampton) screens and then manually optimized. Crystals of 8ANC195 Fab (space group $P4_12_12$, a = 66.5 Å, b = 66.5 Å, c = 219.0 Å; one molecule per asymmetric unit) were obtained upon mixing a protein solution at 11 mg/mL with 0.1M Hepes pH 7, 20% PEG 6,000, 10 mM zinc chloride at 20°C. Crystals were briefly soaked in mother liquor solution supplemented with 20% ethylene glycol before flash cooling in liquid nitrogen. Crystals of the 8ANC195 Fab/93TH057 gp120/sCD4$_{K75T}$ complex (space group $P2_12_12_1$, a = 66.5 Å, b = 132.5 Å, c = 142.8 Å; one molecule per asymmetric unit) were obtained upon mixing a protein solution at 16 mg/mL with 14% polyethylene glycol 3,350, 0.1 M HEPES pH 7.3, 2% benzamidine HCl at 20°C. Crystals were briefly soaked in mother liquor solution supplemented with 30% ethylene glycol before flash cooling in liquid nitrogen.

Crystallographic data collection, structure solution and refinement

X-ray diffraction data for 8ANC195 Fab crystals were collected at the Argonne National Laboratory Advanced Photon Source (APS) beamline 23-ID-D using a MAR 300 CCD detector. X-ray diffraction data for 8ANC195 Fab/93TH057 gp120/sCD4$_{K75T}$ complex crystals were collected at the Stanford Synchrotron Radiation Lightsource (SSRL) beamline 12-2 using a Pilatus 6M pixel detector (Dectris). The data were indexed, integrated and scaled using XDS (Kabsch, 2010).

The 8ANC195 Fab structure was solved by molecular replacement using Phenix (Adams et al., 2010) and the V_HV_L and C_H1C_L domains of NIH45-46 Fab (PDB code 3U7W) lacking all CDR loops as two separate search models. The model was then refined to 2.13 Å resolution using an iterative approach involving refinement and verification of model accuracy with simulated annealing composite omit maps using the Phenix crystallography package (Adams et al., 2010), and manually fitting models into electron density maps using Coot (Emsley and Cowtan, 2004). The final model (R_{work} = 20.2%; R_{free} = 24.2%) includes 3,321 protein atoms, 15 ligand atoms and 178 water molecules (Table S1). 99.54%, 0.46% and 0.0% of the residues were in the favored, allowed and disallowed regions, respectively, of the Ramachandran plot. Disordered residues that were not included in the model include residues 127-134, 214-219 and the 6x-His tag of the 8ANC195 heavy chain, and residues 213-214 of the light chain.

The 8ANC195 Fab/93TH057 gp120/$sCD4_{K75T}$ complex structure was solved by molecular replacement using Phaser (Adams et al., 2010) and the V_HV_L and C_H1C_L domains of 8ANC195 (lacking all CDR loops), 93TH057 gp120 (taken from PDB code 3U7Y), and sCD4 (taken from PDB code 3LQA) as separate search models. The complex structure was refined to 3.0 Å resolution as described for the Fab structure. In addition to considering I/σ_I and completeness of the highest resolution shell (2.1% and 99.9%, respectively), we used the $CC_{1/2}$ statistic (Karplus and Diederichs, 2012) (correlation coefficient between two random halves of the data set where $CC_{1/2}$ > 10%) to determine the high-resolution cutoff for our data. Phenix (Adams et al., 2010) was used to compute $CC_{1/2}$ (85.4% for the highest resolution shell and 99.8% for the entire data set), supporting our high-resolution cutoff determination.

The final model (R_{work} = 23.5%; R_{free} = 27.2%) includes 7195 protein atoms and 408 atoms of carbohydrates and ligands (Table S1). 96.92%, 3.08% and 0.0% of the residues were in the favored, allowed and disallowed regions, respectively, of the Ramachandran plot. Disordered residues that were not included in the model include residues 126-135, 185-194,

214-219 and the 6x-His tag of the 8ANC195 heavy chain, residues 212-214 of the light chain, residues 125-197 (V1/V2 substitution), 302-324 (V3 substitution), residues 396-408 (a total of 6 residues from V4), residues 492-494 and the 6x-His tag of 93TH057 gp120 and residues 106-111, 150-152, 178-186 and the 6x-His tag of $sCD4_{K75T}$.

Buried surface areas were calculated using PDBePISA (Krissinel and Henrick, 2007) and a 1.4 Å probe. Superimposition calculations were done and molecular representations were generated using PyMOL (Schrödinger, 2011). Pairwise Cα alignments were performed using PDBeFold (Krissinel and Henrick, 2004).

Isolation of 8ANC195 variants

Single Cell clonal variants of 8ANC195 were isolated by 2CC core-specific single cell sorting, followed by reverse transcription and immunoglobulin gene amplification as described previously (Scheid et al., 2011). Immunoglobulin genes were cloned into heavy and light chain expression vectors and co-transfected for IgG production as described previously (Tiller et al., 2008).

IgG+ CD19+ memory B cells were bulk sorted on a FACS AriaIII cell sorter. Bulk mRNA was extracted using TRIzol (Invitrogen) and reverse transcribed as previously described (Scheid et al., 2011). 8ANC195-related heavy and light chain genes were PCR amplified using the following clone-specific primers:

For heavy chain amplification: 5' GGTGTACATTCTCAGATACACCTCGTACAA 3' and

5' CAGGTGTCCAGTCTCAGATACA 3' as forward primers and

5' GCGGAGACGGAGATGAGGGTT 3' as a reverse primer. For light chain amplification:

5' GACATCCAGATGACCCAGTCTCCTTCCACCCTGTCTGCATCTATAGGT 3' and

5' GACATCCAGATGACCCAGTCTCCTTCCACCCTGTCTGCATCT 3' as forward and

5' GTTTCACCTCAACTTTAGTCCCTT 3' as well as

5' GTTTCACCTCAACTTTAGTCCCTTGGCCGAAGGTC 3' as reverse primers.

Amplification products were gel purified and cloned into TOPO TA sequencing vectors (Invitrogen) and expression vectors as described previously (Tiller et al., 2008).

Supplemental References

Adams, P.D., Afonine, P.V., Bunkoczi, G., Chen, V.B., Davis, I.W., Echols, N., Headd, J.J., Hung, L.W., Kapral, G.J., Grosse-Kunstleve, R.W.*, et al.* (2010). PHENIX: a comprehensive Python-based system for macromolecular structure solution. Acta Crystallogr D Biol Crystallogr *66*, 213-221.

Emsley, P., and Cowtan, K. (2004). Coot: model-building tools for molecular graphics. Acta Crystallogr D Biol Crystallogr *60*, 2126-2132.

Julien, J.P., Cupo, A., Sok, D., Stanfield, R.L., Lyumkis, D., Deller, M.C., Klasse, P.J., Burton, D.R., Sanders, R.W., Moore, J.P.*, et al.* (2013). Crystal Structure of a Soluble Cleaved HIV-1 Envelope Trimer. Science.

Kabsch, W. (2010). Integration, scaling, space-group assignment and post-refinement. Acta Crystallogr D Biol Crystallogr *66*, 133-144.

Karplus, P.A., and Diederichs, K. (2012). Linking crystallographic model and data quality. Science *336*, 1030-1033.

Krissinel, E., and Henrick, K. (2004). Secondary-structure matching (SSM), a new tool for fast protein structure alignment in three dimensions. Acta Crystallogr D Biol Crystallogr *60*, 2256-2268.

Krissinel, E., and Henrick, K. (2007). Inference of macromolecular assemblies from crystalline state. J Mol Biol *372*, 774-797.

Lyumkis, D., Julien, J.P., de Val, N., Cupo, A., Potter, C.S., Klasse, P.J., Burton, D.R., Sanders, R.W., Moore, J.P., Carragher, B.*, et al.* (2013). Cryo-EM Structure of a Fully Glycosylated Soluble Cleaved HIV-1 Envelope Trimer. Science.

Scheid, J.F., Mouquet, H., Ueberheide, B., Diskin, R., Klein, F., Olivera, T.Y., Pietzsch, J., Fenyo, D., Abadir, A., Velinzon, K.*, et al.* (2011). Sequence and Structural Convergence of Broad and Potent HIV Antibodies That Mimic CD4 Binding. Science *333*, 1633-1637.
Schrödinger, L. (2011). The PyMOL Molecular Graphics System (The PyMOL Molecular Graphics System).

Tiller, T., Meffre, E., Yurasov, S., Tsuiji, M., Nussenzweig, M.C., and Wardemann, H. (2008). Efficient generation of monoclonal antibodies from single human B cells by single cell RT-PCR and expression vector cloning. J Immunol Methods *329*, 112-124.